Available online at www.sciencedirect.com
SCIENCE DIRECT®
International Journal of Heat and Mass Transfer 49 (2006) 1320–1328
International Journal of HEAT and MASS TRANSFER
www.elsevier.com/locate/ijhmt

# Conjugate heat transfer measurements with single-phase and water flow boiling in a single-side heated monoblock flow channel

Ronald D. Boyd *, Hongtao Zhang

*Thermal Science Research Center, College of Engineering, Prairie View A&M University, P.O. Box 4208, Prairie View, TX 77446-4208, USA*

Received 15 April 2005; received in revised form 7 October 2005
Available online 20 December 2005

**Abstract**

Optimized and robust designs of one-side heated plasma-facing components and other heat flux removal components are dependent on conjugate heat transfer. In the present case, the conjugate heat transfer involved measuring the local distributions of the inside wall temperature and heat flux in a single-side heated monoblock flow channel with: (1) peripheral (radial and circumferential) heat transfer; and, (2) coupled internal turbulent, forced convective single-phase flow and flow boiling. For the first time, multi-dimensional boiling curves have been measured for a single-side heated monoblock flow channel. Using a thermal hydraulic diameter as the characteristic dimension in select correlations for the highest mass velocity (3.2 $Mg/m^2$ s), good agreement was obtained. At lower mass velocities, only the single-phase correlations agreed better with the data for the averaged net incident heat flux vs the inside channel wall temperature. Hence, additional correlation development and adaptation are needed for single-side heated monoblocks with peripheral heat transfer.


*Keywords:* Single-side heated monoblock; Conjugate heat transfer measurements; 2-D Water flow boiling curves

## 1. Introduction

Many engineering applications involve conjugate heat transfer in substrates which: (1) are heated from a single side; (2) are cooled via coupled, internal, turbulent single-phase or two-phase flow; and, (3) have peripheral or circumferential heat transfer around the flow channel. Examples include plasma-facing components (PFCs) in fusion reactors, optical heat sinks, electronic heat sinks, protective air transport systems, and space systems. In some high heat flux removal systems, the internally flowing fluid likely may change phase along the length of the flow channel. Engineering feasibility studies and reviews (e.g., [1,2]) have shown the advantages of and the need for local embedded thermocouple data for characterizing conjugate heat transfer in applications involving single-side heated components with both internal and circumferential cooling. Such data would be invaluable in the future scale-up activity to large-scale components and applications. For optimized and robust system development where single-side heat transfer is involved, it is necessary to measure, understand and, correlate the non-uniform or single-side heating effects on the resultant inside flow channel heat flux and temperature distributions (i.e., the boiling curve).

The objective of the present work was to produce two-dimensional (2-D) boiling curves using steady-state, three-dimensional (3-D), flow boiling and single-phase measurements in a horizontal single-side heated monoblock flow channel with water as a flowing fluid. The purposes of this experimental investigation were to: (1) measure the local 3-D wall temperature distributions for a given net applied heat flux; (2) use the wall temperature measurements to extrapolate the 2-D temperature distribution on the inside wall of the flow channel; (3) estimate the 2-D inside channel wall heat flux distributions; and, (4)

* Corresponding author. Tel.: +1 936 857 4811; fax: +1 936 857 4858.
*E-mail address:* ronald_boyd@pvamu.edu (R.D. Boyd).

0017-9310/$ - see front matter © 2005 Elsevier Ltd. All rights reserved.
doi:10.1016/j.ijheatmasstransfer.2005.10.010

**Nomenclature**

| | |
|---|---|
| $a$ | parameter for the thermal hydraulic diameter |
| $A_c$ | cross section area of flow channel, $m^2$ |
| $D_i$ | flow channel inside diameter, m |
| $D_T$ | thermal-hydraulic diameter $D_T = aD_i$, m |
| $G$ | mass velocity, $kg/m^2$ s |
| $i$ | specific enthalpy, kJ/kg |
| $i_{fg}$ | specific latent heat of vaporization, kJ/kg |
| $k$ | thermal conductivity of test section (TS), W/m K |
| $k_f$ | thermal conductivity of the fluid, W/m K |
| $L$ | heated length of the flow channel, m |
| $L_i$ | unheated inlet portion of the flow channel, m |
| $L_o$ | unheated outlet portion of the flow channel, m |
| $Nu$ | Nusselt number with temperature dependent properties evaluated at the local film temperature |
| $Nu_o$ | Nusselt number with temperature dependent properties evaluated at the local bulk fluid temperature |
| $P$ | exit pressure, MPa |
| $q_o$ | net rate of thermal energy transferred to the fluid in the TS, kW |
| $q''$ | heat flux, $kW/m^2$ |
| $q''_i$ | 2-D ($\phi$ and $Z$) flow channel inside wall heat flux (also referred to as Inside HF), $kW/m^2$ |
| $q''_o$ | averaged, net incident heat flux (also referred to as incident HF), which is equal to the ratio of $q_o$ to the outside heated surface area ($Lw$) of the TS, $kW/m^2$ |
| $q''_{oo}$ | incident heat flux, $kW/m^2$ |
| $r$ | radial coordinate of the TS, m |
| $r_i$ | inside radius of the flow channel, m |
| $r_o$ | outside radius (and a function of $\phi$) of the test section, m |
| $r_1$ | radial location of embedded thermocouple closest to the inside radius of the flow channel, m |
| $Re$ | Reynolds number, $\frac{GD_i}{\mu}$ |
| $T$ | temperature, °C |
| $T_b$ | bulk temperature of the fluid, °C |
| $T_f$ | film temperature of the fluid, °C |
| $T_{fdb}$ | onset of fully-developed boiling TS inside wall temperature, °C |
| $T_{ONB}$ | onset of nucleate boiling TS inside wall temperature, °C |
| $T_{sat}$ | saturation temperature of the fluid at the exit pressure of the TS, °C |
| $T_w$ | local wall temperature, °C |
| $T_{wi}$ | inside TS flow channel boundary temperature, °C |
| $T_{w1}$ | measured TS wall temperature at $r = r_1$, °C |
| TS | test section |
| $w$ | heater width, m |
| $w_1$ | test section width, m |
| $Z$ | local axial coordinate with origin at the beginning of the TS heated section (see Fig. 1 for locations of $Z_1 = 0.049$ m, $Z_2 = 0.098$ m, $Z_3 = 0.147$ m, and $Z_4 = 0.196$ m), m |

*Greek symbols*

| | |
|---|---|
| $\mu$ | dynamic viscosity, kg/m s |
| $\phi$ | circumferential coordinate of TS ($\phi = 0$ on the heated side of the TS plane of symmetry; see Fig. 1), degrees |

make comparisons between the experimental data and selected correlations from the literature.

Since the complete experimental system is described elsewhere [3], only a summary of the flow parameters will be given. The flow parameters are as follows: 0–3.0 $MW/m^2$ heat flux, 0.59–3.15 $Mg/m^2$ s mass velocity, 0.21–0.57 MPa exit pressure, $5 \times 10^3$–$2 \times 10^5$ Reynolds number, and less than 130 °C subcooling.

In his review of actively cooled PFCs, Nygren [2] alluded to the importance of monoblock flow channel data from embedded thermocouples. In the case of plasma facing components heated from one side, Araki et al. [1] emphasized the need for a comprehensive database which includes heat transfer around the circumference of flow channels. Using existing uniform heat flux correlations, they compared their data for single-side heated circular cylindrical flow channels ($r_i = 5.0$ mm) as a function of the incident heat flux and local wall temperature. Using Shah's (Jens and Lottes') and Thom's correlations, a modified inverse conduction analysis was compared favorably with local circumferential temperature variations which were recorded from embedded (in the wall of the flow channel) thermocouples. However, no data were produced for the inside flow channel wall temperature ($T_{wi}$) and heat flux ($q_i$). In one case involving a tube without a twisted tape, the local heat transfer coefficient was compared and found to be bracketed by these correlations to within ±30%. Some form of the modified inverse analysis produced predictions for $T_{wi}$ and $q_i$; but, the analysis were based on either the Shah or Thom correlation. It should be noted that conventional inverse conduction analyses should be independent of such correlations. Therefore, there is still a need to produce $T_{wi}(\phi, Z)$ and $q_i(\phi, Z)$ for single-side heated circular and monoblock flow channels with internal single-phase and flow boiling conditions.

In their study, Araki et al. [4] measured local ($r/r_i = 1.3$) circumferential channel wall temperature variations in a single-side heated circular flow channel ($r_o/r_i = 1.5$). One of their objectives was to determine whether existing heat transfer correlations, developed for uniform heating, were

applicable for single-side heated circular flow channels in the single-phase and flow boiling regimes. They concluded that existing correlations: (1) could be used in the "non-boiling region", but (2) could not be used in the subcooled flow boiling regimes. Using a correlational form similar to that of the Thom and Jens-Lottes correlations for the subcooled flow boiling fully-developed regime, they proposed a new correlation which fit (±15%) their single-side heated data base. Consistent with the peaking factor (PF) predictions of Boyd and Meng [5], they found that the PF was less than $r_o/r_i$.

Based on a modified mixing-length turbulent model and the Davis–Anderson onset of nucleate flow boiling (ONB) criterion, Shim et al. [6] used a two-dimensional conjugate analysis for annuli with finite thickness fins to successfully predict (to within 13%) ONB data and wall-to-fluid temperature differences. In addition to including variable fluid properties for their fully-developed (both hydrodynamically and thermally) turbulent flow, comparisons were made with smooth annulus data. For these cases: (1) the ratio of outside to inside flow channel radius varied form 1.6 to 80.7, (2) the Reynolds number varied from $10^4$ to $10^6$, and (3) the Prandtl number varied from 0.7 to 10.0. The ONB was computed as the intersection of two curves formed by the Davis–Anderson criterion and that at the fluid–solid interface from the conjugate analysis. Very good agreement resulted up to a mean velocity of 4.0 m/s. In all cases, the ONB occurred at the center of the root between two fins.

Increasing international attention is being given to single-side heated flow channels which might be used in PFCs and other applications. Using the ABAQUS code and unspecified swirl flow boiling correlations, Youchison et al. [7] obtained good agreement with data for a single-side heated monoblock with internal water flow boiling. Raffray et al. [8] addressed three different coolant systems for single-side heat flux accommodation in future fusion reactor divertor and blanket components. Among other details, they noted that "structural integrity" requires the monoblock pitch to be $\geqslant$20.0 mm for a 10.0 mm inside diameter flow channels. For this channel size, the PF was estimated to be 1.46 for a pitch of 19.0 mm and 1.6 when the pitch is 24.0 mm. Obviously, PF also depends on the value of $\frac{r_o-r_i}{r_i}$ at $\phi = 0$. Baxi [9] reviewed and summarized important aspects of heat transfer in single-side heated monoblocks used in PFCs which included: (1) a typical variation of the heat transfer coefficient over all subcooled flow boiling regimes, (2) a typical ratio of inside flow channel wall heat flux to the incident heat flux ($\lesssim$1.5) for flow channels with swirl tape inserts, and (3) a summary assessment of various heat transfer enhancement techniques. For single-side heated flow channels with swirl tape inserts, Inasaka and Nariai [10] studied the circumferential heat flux variation and developed correlations for single-side heat flux multipliers relative to uniformly heated flow channels. Among many important issues, the design of PFCs depends on resulting thermal stresses which result when composite monoblocks are subjected to heat fluxes from one side [11]. Embedded temperature measurement results will assist in this regard. Razmerov and Molochnikov [12] studied stability of fusion reactor first wall flow channels for inlet and flow conditions recommended by Raffray et al. [8]. Under these conditions, they found that stability became an important issue when the monoblock mass velocity was substantially reduced. It appears that additional work is still needed on stability issues for PFCs.

Izumi et al. [13] studied heat transfer mechanisms based on temperature profiles and bubble motion from a single-side heated copper block on a test section with internal flow boiling but without peripheral or circumferential cooling. Although this and other such studies (e.g., [14]) contain fundamental flow boiling phenomenology, the test sections used significantly differ from the present single-side heated monoblock because of the absence of circumferential heat transfer.

## 2. Test section

A schematic of the monoblock test section is shown in Fig. 1. Fabricated from Type AL-15 Glidcop Grade Copper, its overall length, including the inlet and outlet reduced diameter sections, is 360.0 mm. The main section of the test section (available for heating) is 200.0 mm long with a nominal outside surface width of the square cross section monoblock of 30.0 mm and an inside diameter of 10.0 mm. The test section was heated from a single side with an electrically-isolated graphite heater (see [3]). For these tests, the actual directly heated length, $L$, was 180.0 mm. Thermocouples (0.5 mm O.D. stainless steel sheathed, Type-J) were placed in 48 thermal well locations inside the solid portion of the monoblock. For each of four axial ($Z$-) stations, thermocouples were embedded at three radial and four circumferential locations (0°, 45°, 135°, and 180°). The thermocouples were calibrated to within 0.1 °C with a precision calibrator.

The purpose of the four axial locations is to obtain an estimate of the axial distribution of the test section wall temperature for a given applied heat flux. Shown in the figure are four axial stations at axial locations $Z_1$, $Z_2$, $Z_3$, and $Z_4$. These are locations where thermocouple (TC) wells exist for local in-depth wall temperature measurements. Since the geometry of the TC wells is identical at all four primary axial stations, a detail description will be given for only one axial station. For example, the $A$–$A$ axial station at $Z_4$ has twelve (12) TC wells, with ten (10) wells in plane $A1$ and one each in planes $A2$ and $A3$ which are axially displaced upstream from plane $A1$ by 2.0 mm and 4.0 mm, respectively. The thermocouples at station $A$–$A$ will give both radial and circumferential distributions of the local wall temperature. A combination of all axial stations will produce a three-dimensional distribution of the test section local wall temperature as a function of the applied heat flux. Depending on the heat flux level,

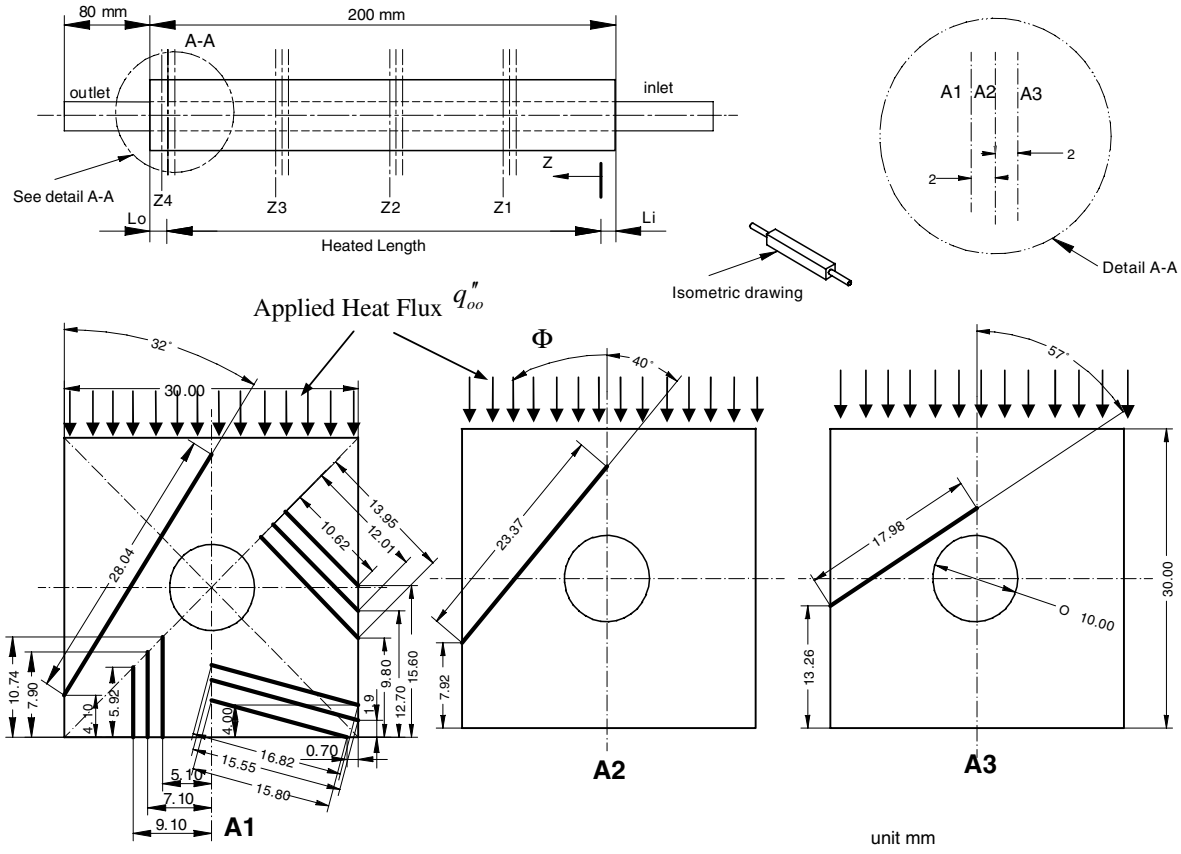


Fig. 1. Monoblock test section (TS) used for local temperature and heat transfer measurements. Water flows through the 10.0 mm inside diameter channel. The thermocouple (TC) wells are the solid black lines with specified lengths and angles.

the water convective turbulent flow regime will vary from single-phase at the inlet to subcooled flow boiling (at higher heat flux levels) near the exit.

Included in the data reduction is data corrections due to the axial location and data extrapolation to the inside flow channel boundary. In the test section for each nominal axial location, three different planes (i.e., planes $A1$, $A2$, and $A3$ in Fig. 1) have embedded thermocouples. At $\phi = 0°$ for example, the $A$-plane thermocouple which is: (1) close to the fluid is in plane $A3$ or at an axial location of $Z_4$— 4 mm, and (2) at the intermediate radial location is between the TC close to fluid and the TC close to the outside boundary and is located at an axial location of $Z_4$— 2 mm. All the data from these two planes (or analogous planes) were corrected to the $Z_4$ location (or at other analogous locations, e.g., $Z_1$, $Z_2$, or $Z_3$) using a linear interpolation over a distance of 2 or 4 mm between axial TC measurements which were 49 mm apart. So, the correction distance for the axial location is a small percentage (<8.2%) of the axial TC separation. Local wall temperature measurements at the three radial locations were used to extrapolate the inside flow channel wall temperature ($T_{wi}(\phi, Z) = T_w(r = r_i, \phi, Z)$).

The inside flow channel wall heat flux was calculated using a local thermal conduction equation from the measured wall temperatures close to the fluid location ($T_{w1}$ @ $r = r_1$) and the extrapolated inside flow channel wall temperatures ($T_{wi}$ @ $r = r_i$); i.e.,

$$q''_i = k\frac{\Delta T}{\Delta r} = k\frac{(T_{w1} - T_{wi})}{r_1 - r_i}, \tag{1}$$

where $k$ is the local temperature-dependent thermal conductivity of the TS. Using data from the manufacturer [15] of the Glidcop copper test section material, the following equation was obtained for the temperature dependence of $k$,

$$k = -\frac{3}{25}T + 367.4, \tag{2}$$

where $k$ is in W/m K, and $T$ (in °C) is the local wall temperature. In Eq. (1), the thermal conductivity of the monoblock test section was evaluated at the mean value of the inside flow channel wall temperature $T_{wi}$ and the measured wall temperature ($T_{w1}$) close to the fluid location.

## 3. Monoblock thermal boundary conditions

The thermophysical configuration for the monoblock test section is shown in Fig. 2. The incident heat flux was applied to a single-side and subcooled water flowed through the channel in the center of the test section. A flow-developing section existed upstream of the heated

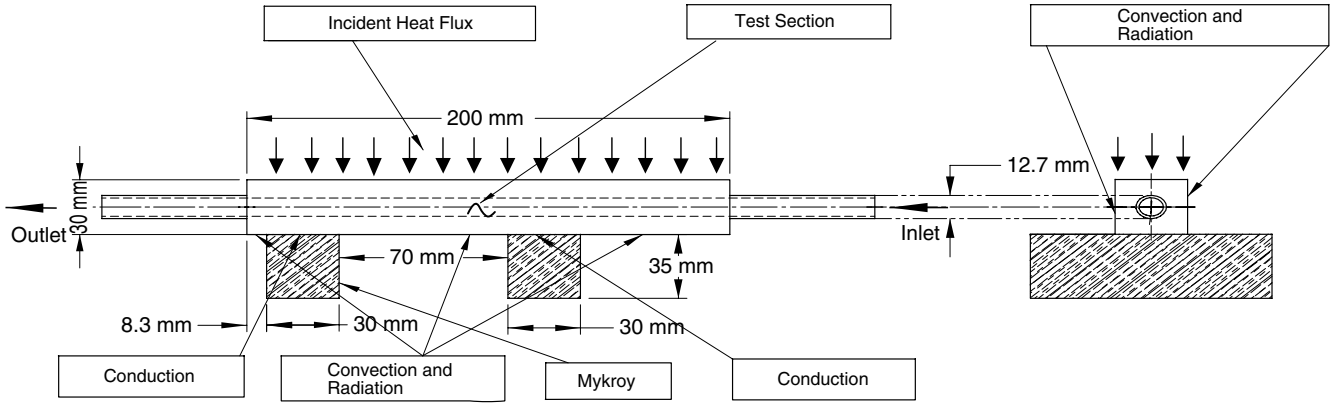


Fig. 2. Boundary conditions for the monoblock test section (see Fig. 1).

section such that the flow in the heated section was hydrodynamically fully-developed. The test section was exposed to ambient air on all other surfaces except on the top (where the incident heat flux was applied) and where the mykroy ($k = 1.32$ W/m K) supports were located on the bottom. This resulted in heat losses from the test section due to the natural convection, radiation and conduction to the surroundings. In addition, there were energy losses via axial conduction to the flow loop. The total rate of heat losses to the surroundings were estimated to be less than 1.5% of the rate of energy transferred to the flowing fluid (i.e., $q_o$). The averaged net incident heat flux ($q''_o$) was computed from the ratio of $q_o$ to the product of $Lw$ ($= A_s$). Thus, $q''_o$ is given by

$$q''_o = \frac{\dot{m}(i_2 - i_1)}{A_s}, \tag{3}$$

where $\dot{m}$ is the mass flow rate in kg/s; $i_1$ and $i_2$ are the inlet and outlet water specific enthalpies, respectively; and $A_s$ is the surface area of the test section–heater interface. The local ($Z$-location) bulk specific enthalpy was calculated from $q''_o$ and the inlet water specific enthalpy using an equation similar to Eq. (3) or

$$i_l = i_1 + \frac{q''_o \cdot w \cdot Z}{\dot{m}}, \tag{4}$$

where, $i_l$ is the local bulk specific enthalpy at the $Z$-location, $w$ is the heated width of the test section, and $Z$ is the axial distance from the inlet heated point of the test section. Then, the local bulk temperature was interpolated from thermodynamic data using the local bulk specific enthalpy ($i_l$). It was used in some heat transfer correlations for comparisons with the measured data.

In the present work, single-side heating effects were accounted for by replacing $D_i$ as the characteristic diameter in some correlations with the thermal-hydraulic flow diameter [16,17],

$$D_T = a \cdot D_i, \tag{5}$$

where $a$ is a parameter, and $D_i$ is the test section inside flow diameter. The quantity $D_T$ was used to: (1) predict the onset nucleate boiling heat flux and fully developed boiling heat flux for the single-side heated test section, and (2) in select boiling curve correlations. It should be noted that $D_T$ was used only in the Reynolds number ($Re_{D_T}$) and the Nusselt number ($Nu_{D_T}$).

## 4. Results

The three-dimensional (3-D) temperature distributions were measured as a function of the averaged net incident flux ($q''_o$) for the single-side heated monoblock test section which is cooled internally via single-phase convection and flow boiling (see Figs. 1 and 2). All local measurements include effects of conjugate heat transfer with turbulent flow. The measurements were used to radially extrapolate the inside flow channel wall temperature ($T_{wi}$) and then determine the inside heat flux ($q''_i$). These results are the first direct representation of 2-D boiling curves for a single-side heated monoblock. Comparisons with selected correlations from the literature were made.

Since there appears to be few correlations in the literature (e.g., see [4,16]) developed for a single side heated flow channel, selected correlations and methodologies (e.g., [4,18,19]), which have been applied to a single side heated flow channel, were compared with the present data. In the Marshall et al. methodology [18], the following single-phase and subcooled flow boiling correlations were used: (1) Sieder–Tate for the single-phase region, (2) Bergles–Rohsenow for the onset of nucleate boiling, (3) Bergles–Rohsenow for the partial nucleate boiling regime, and (4) Araki et al. [4] for the fully-developed boiling regime. In reporting their correlation for the fully-developed nucleate boiling regime, Araki et al. used the same correlation to obtain agreement (±15%) with flow channels with and without a swirl tape insert. Although Marshall et al. used the arithmetic mean bulk temperature based on the inlet and outlet bulk temperatures for their single axial measurement location, the predictions in the present work use the local bulk temperature, $T_b(Z)$ for the multiple axial measurement locations. In the Boyd–Meng methodology [19], the following single-phase and subcooled flow

boiling correlations were used: (1) Petukhov for the single-phase regime, (2) Bergles-Rohsenow for the onset of nucleate boiling, (3) Boyd–Meng correlation for the partial nucleate boiling regime, (4) Engelberg–Forster–Greif criterion for the onset of fully-developed boiling, and (5) Shah for the fully-developed boiling regime.

### 4.1. Boiling curves

The applied power from the test section heater [3] was used to generate the incident heat flux, $q''_{oo}$ (see Fig. 1). This heat flux was varied so that the test section flow ranged from single-phase to well into the fully-developed, nucleate flow boiling regime. In all cases, flow rate, average net incident heat flux ($q''_o$), and exit pressure were parameters for these steady-state experiments. Local (3-D) wall temperature measurements were made and used to determine the 2-D distributions for the flow channel inside: (1) wall temperature, (2) heat flux, and (3) the resulting boiling curves.

From the embedded thermocouples in the single-side heated test section, a set of sixteen (16) inside flow channel wall temperatures ($T_{wi}$) and the inside wall heat fluxes ($q''_i$) were obtained for different levels of the average net incident heat flux, $q''_o$. These sets include four axial ($Z_1 = 49.02$ mm, $Z_2 = 98.04$ mm, $Z_3 = 147.07$ mm, and $Z_4 = 196.09$ mm) and four circumferential ($\phi = 0°$, 45°, 135°, and 180°) locations. In Fig. 3a through d, the locus of the "star" symbol data points represents the boiling curves (i.e., $q''_i$ vs $T_{wi}$ with $T_{sat}$ included) for a mass velocity of 0.59 Mg/m$^2$ s and exit pressure of 0.207 MPa at: (1) an axial location

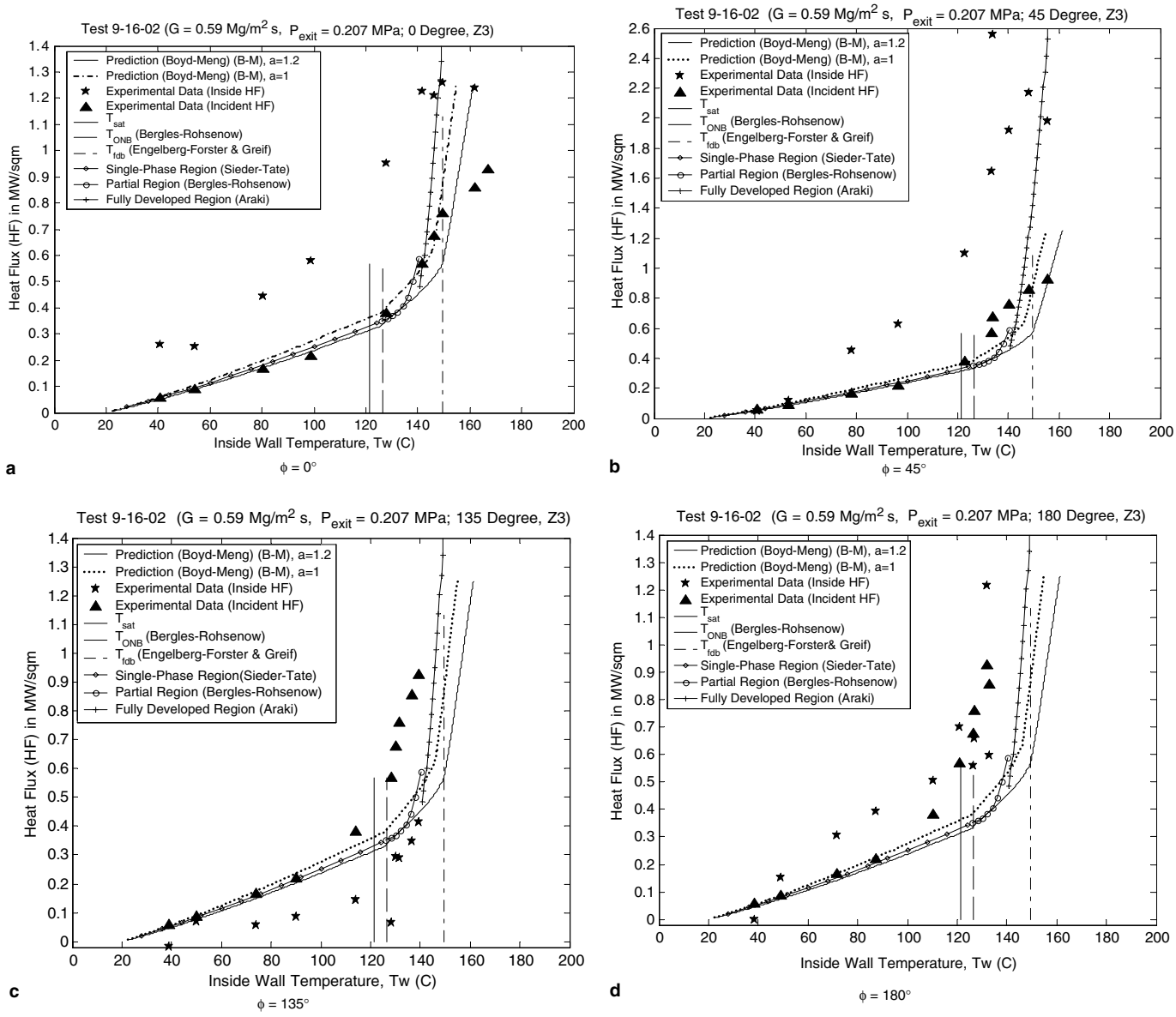


Fig. 3. Selected correlation comparisons with data for flow channel wall inside heat flux and averaged net incident heat flux as a function of the inside flow channel ($D_i = 10.0$ mm) wall temperature at four circumferential locations [(a) $\phi = 0°$, (b) $\phi = 45°$, (c) $\phi = 135°$, and (d) $\phi = 180°$] for a mass velocity of 0.59 Mg/m$^2$ s, exit pressure of 0.207 MPa, an axial location of $Z_3 = 147.1$ mm, and a heated length of 180.0 mm.

of 147.07 mm (about three-quarters downstream of the heated entrance), and (2) the four circumferential locations. The first vertical line denotes the saturation temperature at the exit pressure. The "triangular" symbol data points represent $q''_o$ vs $T_{wi}$. The ratio of $q''_i$ to $q''_o$ is related to the local peaking factor. To enhance data interpretation, the onset of nucleate boiling (ONB) inside wall temperature and the onset of fully developed nucleate boiling (FDB) inside wall temperature were computed. These are shown as the remaining two vertical lines in Fig. 3.

Initially as $T_{wi}$ increases, $q''_i$ @ $\phi = 0°$ (Fig. 3a) was greater than $q''_i$ @ $\phi = 45°$ (Fig. 3b). However in the middle to the latter portion of the single-phase region, $q''_i$ @ $\phi = 45°$ became $> q''_i$ @ $\phi = 0°$; and, this continued into the subcooled flow boiling regime. Similar trends occurred at the higher mass velocities of 1.18 and 3.15 Mg/m$^2$ s. Further, inspection and comparisons of Fig. 3a through d ($\phi = 180°$) indicate that the shape of the boiling curve does change as $\phi$ changes. For example, in Fig. 3b ($\phi = 45°$) and 3c ($\phi = 135°$), the corresponding values of $T_{wi}$ are quite different for the same value of $q''_i$. Similar results were produced at all axial locations and the three levels of the mass velocity. These results represent an evolving 2-D conjugate heat transfer and boiling curve data base for a single-side heated monoblock; and hence for the first time, a multi-dimensional boiling curve data base has been measured for a single-side heated monoblock flow channel.

### 4.2. Data/correlation comparisons

The above noted correlations have been used to express a relationship between the inside channel wall heat flux and the inside wall temperature. Although most of the correlations were developed for uniform heat flux, the Araki et al. [4] correlation has been applied to single-side heated flow channel configurations. The single-side heated effect was accounted for in the Boyd–Meng methodology by using $D_T$ (e.g., see [17]) as the characteristic diameter. Since all correlations were developed for thermally and hydrodynamically fully-developed flow, comparisons were made at a down-stream location ($Z = Z_3$ or $Z_3/D_i = 14.7$) where these conditions exist. Fig. 3a through d contain comparisons with the inside heat flux and inside wall temperature (i.e., $q''_i$ vs $T_{wi}$ or "star" symbol) data set at $Z = Z_3 = 147.1$ mm and $G = 0.59$ Mg/m$^2$ s. There is no agreement or correlation with this data; but there is some correlation at higher mass velocities. Since the correlations for the most part were developed for a uniform heat flux flow channel, this poor correlation is not surprising. However, the correlations are closer to the $q''_o$ vs $T_{wi}$ ("triangular" symbol) data set in many cases.

In the single-phase region for $G = 0.59$ Mg/m$^2$ s, the Sieder–Tate correlation and the Boyd–Meng methodology with $a = 1.2$ characterized the $q''_o$ vs $T_{wi}$ relationship for the data fairly well. For this mass velocity, all correlations under-predicted (e.g., see Fig. 4) the inside heat flux for a given value of $T_{wi}$; and at most circumferential locations for the highest mass velocity (3.15 Mg/m$^2$ s), the correlations over-predict the inside wall heat flux. Fig. 4 shows that for $\phi = 0°$ and $Z = Z_3$, the Boyd–Meng methodology characterizes the entire boiling curve for the highest mass velocity ($G = 3.15$ Mg/m$^2$ s) well when $a = 1.2$. Better characterization was obtained (not shown) when $a = 1.4$. However, additional results show that none of the correlations

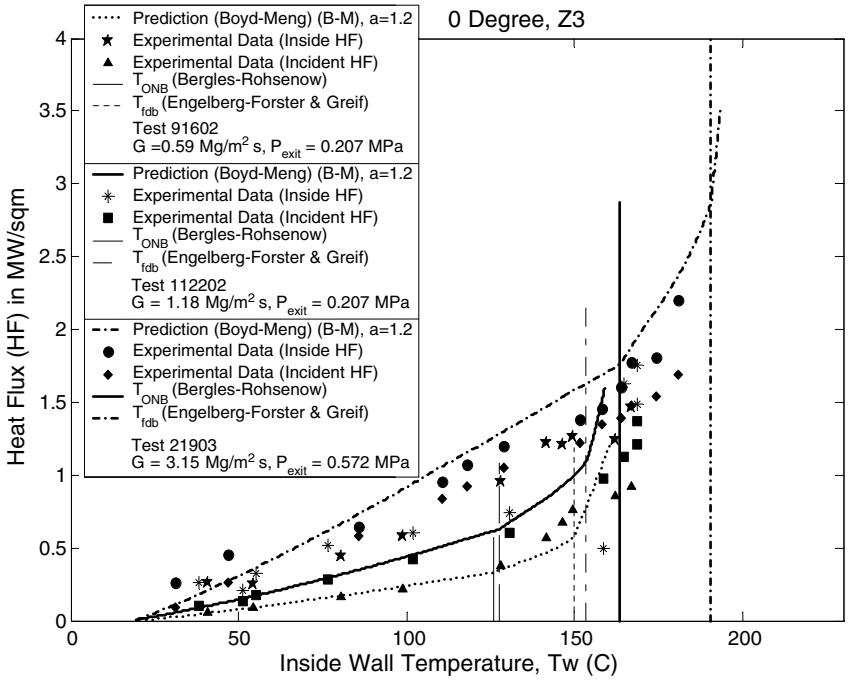


Fig. 4. Select correlation comparisons and mass velocity ($G$) dependence on both the flow channel inside heat flux—and average net incident heat flux—inside wall temperature relationships at $\phi = 0°$ and $Z_3 = 147.1$ mm.

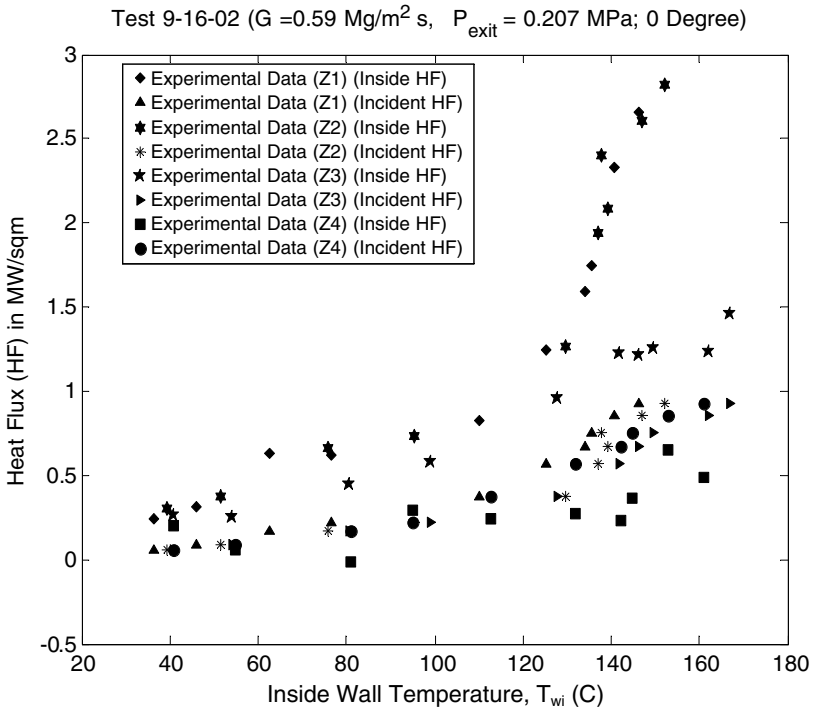


Fig. 5. Axial variation of the $q_i''$ vs $T_{wi}$ and the $q_o''$ vs $T_{wi}$ relationships at $\phi = 0°$ for $G = 0.59$ Mg/m$^2$ s, and $P_{exit} = 0.207$ MPa.

characterized the $q_i''$ vs $T_{wi}$ data at any circumferential coordinates for the two lowest mass velocities ($G = 0.59$ and 1.18 Mg/m$^2$ s). It is therefore apparent that additional work is needed to either adapt existing correlations or develop new correlations which contain single-side and conjugate heat transfer effects for both the turbulent single-phase and flow boiling regimes.

The flow-developing nature of the $q_i''$ vs $T_{wi}$ and $q_o''$ vs $T_{wi}$ relationships are shown as a function of the axial coordinate in Fig. 5 (note: inside HF $= q_i''$ and the incident HF $= q_o''$) at the top (i.e., $\phi = 0°$) of the single-side heated test section. The data base includes similar measurements for other values of $\phi$. The local peaking factor (i.e., PF is related to $q_i''/q_o''$) variation is also apparent; and PF is a function of $Z$, thermal flow developing effects, and the circumferential conjugate heat transfer.

## 5. Conclusions

For the first time, a multi-dimensional boiling curve data base has been developed for a single-side heated monoblock flow channel and it includes effects of: (1) conjugate heat transfer; (2) internal turbulent, single-phase flow and flow boiling; and, (3) circumferential heat transfer. From comparisons with selected correlations, good agreement was obtained only on the heated side of the plane of symmetry: (1) for the entire boiling curve at the highest mass velocity ($G = 3.2$ Mg/m$^2$ s) using the Boyd–Meng correlation with $D_T = 1.4D_i$; and, (2) for the $q_o''$ vs $T_{wi}$ relationship in the single-phase region only at the lower levels of the mass velocity ($G < 1.2$ Mg/m$^2$ s), and using either the Sieder–Tate correlation and the Petukhov correlation with $D_T = 1.2D_i$ (slightly better). Clearly, additional correlation development and adaptation is needed. However, the developed 2-D boiling curve monoblock data base provides a basis for future correlational development so that single-side heating and conjugate heat transfer effects with both circumferential and axial dependence can be correlated.

## Acknowledgements

The authors are appreciative to the Department of Energy (DOE), for its support of this work under contract #DEFG03-97ER54452. They are also appreciative to Mrs. Vivian Davis and Mr. Penrose Cofie, for supporting many aspects of this work. Finally, they are appreciative to Mr. Jonathan Walker for updating Fig. 2.

## References

[1] M. Araki, M. Akiba, R.D. Watson, C.B. Baxi, D.L. Youchison, Data base for thermohydrodynamic coupling with coolants, atomic plasma–material interaction processes in controlled thermonuclear fusion, J. Nucl. Fusion Sci. 5 (1995) 245–265.

[2] R.E. Nygren, Actively cooled plasma facing components for long pulse high power operation, Fusion Eng. Design 60 (2002) 547–564.

[3] R.D. Boyd, P. Cofie, Q. Li, A. Ekhlassi, A new facility for measurements of three-dimensional, local subcooled flow boiling heat flux and related critical heat flux for PFCs, Fusion Sci. Technol. 41 (2002) 1–12.

[4] M. Araki, M. Ogawa, T. Kunugi, K. Satah, S. Suzuki, Experiments on heat transfer of smooth and swirl tubes under one-sided heating conditions, Int. J. Heat Mass Transfer 39 (14) (1996) 3045–3055.

[5] R.D. Boyd, X. Meng, Similarities and differences between single-side and uniform heating for fusion applications–II: sine heat flux, J. Fusion Technol. 27 (1995) 401–407.
[6] S.Y. Shim, H.M. Soliman, G.E. Sims, Turbulent fluid flow, heat transfer and onset of nucleate boiling in annular finned passages, Int. J. Thermal Sci. 39 (2000) 709–720.
[7] D.L. Youchison, J. Schlosser, F. Escourbiac, K. Ezato, M. Ariba, C.B. Baxi, Round robin CHF testing of an ITER vertical target swirl tubes, The 18th IEEE/NPSS Sympos. Fusion Eng. (1999) 385–387.
[8] A.R. Raffray, S. Chiocchio, K. Ioki, D. Krassovski, D. Kubik, R. Tivey, High heat flux thermal-hydraulic analysis of ITER divertor and blanket systems, Fusion Eng. Design 39–40 (1998) 323–331.
[9] C.B. Baxi, Thermal hydraulics of water cooled divertors, Fusion Eng. Design 56–57 (2001) 195–198.
[10] F. Inasaka, H. Nariai, Enhancement of subcooled flow boiling critical heat flux for water in tubes with internal twisted tapes under one-sided-heating conditions, Fusion Eng. Design 39–40 (1998) 347–354.
[11] C.B. Baxi, E.E. Reis, M.A. Ulrickson, P. Heizenroeder, D. Driemeyer, Thermal stress analysis of FIRE divertor, Fusion Eng. Design 66–68 (2003) 323–327.
[12] A.V. Razmerov, Y.S. Molochnikov, Port-limiter and divertor cooling hydraulic stability analysis, Plasma Devices Operat. 8 (2000) 215–224.
[13] M. Izumi, R. Shimada, Heat transfer mechanism based on temperature profiles and bubble motion in microbubble emission boiling, 6th ASME-JSME Thermal Engineering Joint Conference, Hawaii, USA, 2003.
[14] Y. Koizumi, N. Matsishita, H. Ohtake, Experimental examination of triggering mechanism of CHF of sub-cooled flow boiling, 6th ASME-JSME Thermal Engineering Joint Conference, Hawaii, USA, 2003.
[15] SCM Metal Products, Inc., Research Triangle Park, NC 27709.
[16] R.D. Boyd, Single-side conduction modeling for high heat flux coolant channels, Fusion Technol. 35 (1999) 8–17.
[17] Q. Peatiwala, R.D. Boyd Sr., Subcooled flow boiling in circumferentially nonuniform and uniform heated vertical channels with downward flow, J. Heat Transfer 122 (2000) 620–626.
[18] T.D. Marshall, D.L. Youchison, L.C. Caldwallader, Modeling the nukiyama curve for water-cooled fusion divertor channels, Fusion Technol. 39 (2001) 849–855.
[19] R.D. Boyd, X. Meng, Local heat transfer for subcooled flow boiling with water, Fusion Technol. 22 (1992) 501–510.